


How Can an Na⁺ Channel Inhibitor Ameliorate Seizures in Lennox–Gastaut Syndrome?

Yun-Chu Lin, MS,¹ Yi-Chen Lai, MS,² Ping Chou, MS,¹ Shu-Wei Hsueh, MS,^{2,3}
Tien-Hung Lin, BS,¹ Chen-Syuan Huang, PhD,^{2,3} Ren-Wei Wang, MS,¹
Ya-Chin Yang, PhD ,^{2,3,4} and Chung-Chin Kuo, MD, PhD^{1,5}

Objective: Lennox–Gastaut syndrome (LGS) is an epileptic encephalopathy frequently associated with multiple types of seizures. The classical Na⁺ channel inhibitors are in general ineffective against the seizures in LGS. Rufinamide is a new Na⁺ channel inhibitor, but approved for the treatment of LGS. This is not consistent with a choice of antiseizure drugs (ASDs) according to simplistic categorical grouping.

Methods: The effect of rufinamide on the Na⁺ channel, cellular discharges, and seizure behaviors was quantitatively characterized in native neurons and mammalian models of epilepsy, and compared with the other Na⁺ channel inhibitors.

Results: With a much faster binding rate to the inactivated Na⁺ channel than phenytoin, rufinamide is distinctively effective if the seizure discharges chiefly involve short bursts interspersed with hyperpolarized interburst intervals, exemplified by spike and wave discharges (SWDs) on electroencephalograms. Consistently, rufinamide, but not phenytoin, suppresses SWD-associated seizures in pentylenetetrazol or AY-9944 models, which recapitulate the major electrophysiological and behavioral manifestations in typical and atypical absence seizures, including LGS.

Interpretation: Na⁺ channel inhibitors shall have sufficiently fast binding to exert an action during the short bursts and then suppress SWDs, in which cases rufinamide is superior. For the epileptiform discharges where the interburst intervals are not so hyperpolarized, phenytoin could be better because of the higher affinity. Na⁺ channel inhibitors with different binding kinetics and affinity to the inactivated channels may have different antiseizure scope. A rational choice of ASDs according to in-depth molecular pharmacology and the attributes of ictal discharges is advisable.

ANN NEUROL 2021;89:1099–1113

Lennox–Gastaut syndrome (LGS) is an epileptic encephalopathy characterized by cognitive impairment, behavioral disorders, and multiple types of seizures. The seizures could involve different levels of impaired consciousness (eg, atypical absence), tonic/clonic/myoclonic convulsions or jerks, drop or atonic attacks, and automatisms.^{1–3} The electroencephalogram (EEG) patterns are diverse, including focal or diffuse/generalized, fast or slow, and spike/polyspike or spike and wave discharges (SWDs), with SWDs being the hallmark of LGS.⁴ The SWDs in LGS are also called slow SWDs, because they

are usually slower (~1–3Hz), more diffuse, and less rhythmic if compared to the rhythmic generalized 3Hz ones in petit mal absence seizures.^{1,3} The electrophysiological and behavioral seizures in LGS, however, are notorious for the intractability, with progressive cognitive or intellectual decline.² Many classical and new antiseizure drugs (ASDs) have been applied to treat seizures in LGS, including lamotrigine, valproic acid, topiramate, clobazam, and felbamate, but with only limited success.^{3,5} It is of note that except for lamotrigine, the classic Na⁺ channel inhibitors (such as phenytoin and carbamazepine)

View this article online at [wileyonlinelibrary.com](https://www.wileyonlinelibrary.com). DOI: 10.1002/ana.26068

Received Aug 3, 2020, and in revised form Feb 23, 2021. Accepted for publication Mar 14, 2021.

Address correspondence to Dr Yang, Department of Biomedical Sciences, Chang Gung University, 259 Wen-Hwa 1st Road, Kwei-Shan, Tao-Yuan 333, Taiwan; E-mail: ytsyang@mail.cgu.edu.tw or Dr Kuo, Department of Physiology, National Taiwan University College of Medicine, and Department of Neurology, National Taiwan University Hospital, 1 Jen-Ai Road, 1st Section, Taipei 100, Taiwan; E-mail: chungchinkuo@ntu.edu.tw

From the ¹Department of Physiology, National Taiwan University College of Medicine, Taipei, Taiwan; ²Department of Biomedical Sciences, College of Medicine, Chang Gung University, Tao-Yuan, Taiwan; ³Graduate Institute of Biomedical Sciences, College of Medicine, Chang Gung University, Tao-Yuan, Taiwan; ⁴Neuroscience Research Center, Chang Gung Memorial Hospital, Linkou Medical Center, Tao-Yuan, Taiwan; and ⁵Department of Neurology, National Taiwan University Hospital, Taipei, Taiwan

are ineffective against, or could even aggravate, seizures in LGS.^{6,7} More recently, cannabidiol and rufinamide were approved for the treatment of LGS, with a responder rate of ~40% or slightly higher,^{8–15} and rufinamide has been demonstrated to act also as an Na⁺ channel inhibitor.¹⁶ It is intriguing that rufinamide could be especially effective against seizures in LGS, and lamotrigine may have some beneficial effect, but the other members of the same pharmacological category are generally ineffective.

Na⁺ channels are closed (in the resting state) at resting membrane potentials, and opened and then “inactivated” upon membrane depolarization. The inactivated channel is no longer available for the generation of Na⁺ currents and cellular activities, and must be recovered to the resting state with membrane repolarization to be available again. All major anti-seizure Na⁺ channel inhibitors in current clinical practice, from phenytoin to rufinamide, are inactivation stabilizers, which selectively bind to the inactivated rather than the resting states, prohibiting recovery from inactivation and decreasing neuronal activities.^{17–19} The critical pharmacological differences responsible for the different clinical effects among the Na⁺ channel inhibitors therefore are more likely quantitative than qualitative. We have previously characterized that phenytoin, carbamazepine, and lamotrigine all bind slowly (binding rate constants ~1–4 × 10⁴ M⁻¹ s⁻¹) to the fast inactivated state of the Na⁺ channel rather than the resting state.^{20–23} The slow binding kinetics necessitate prolonged periods of depolarization or burst discharges (longer than those in most normal conditions) for adequate drug binding. The inhibitory effect of these classical Na⁺ channel inhibitors is therefore use-dependent and tends to spare normal discharges. On the other hand, this quantitative attribute also explains the ineffectiveness of these classical Na⁺ channel inhibitors on seizure discharges in petit mal absence, myoclonic epilepsy, and LGS,^{6,7,17,19} which are characterized by SWDs or short spikes on EEG. Such EEG patterns are indicative of short burst or depolarization (too short to allow enough drug binding) followed by a long interburst hyperpolarization phase, where most Na⁺ channels are recovered from inactivation and drug binding is negligible. An intuitive way for an Na⁺ channel inhibitor to have a significant suppressive effect on the short bursts in SWDs then is acceleration of binding kinetics. Here we demonstrate that rufinamide is distinct in its ultrafast binding rate (~2.7 × 10⁵ M⁻¹ s⁻¹) to the inactivated Na⁺ channel, and thus has a strong suppressive effect on short neuronal burst discharges associated with SWDs and behavioral seizures in LGS.

Materials and Methods

Preparation of Acute Mouse Hippocampal Slices

C57BL/6 mice used in this study were purchased from BioLASCO (Taipei, Taiwan) or the Laboratory Animal Center of

National Taiwan University College of Medicine (Taipei, Taiwan). Animals were maintained in a vivarium with a controlled 12-hour dark/light cycle with free access to water and food. For brain slice preparation, the brain was obtained from C57BL/6 mice of both sexes and aged postnatal day (p) 19 to 25 (or aged p7–p14 for the acute AY-9944 model, or aged p30–p40 for the pentylenetetrazol [PTZ] model) under isoflurane anesthesia and put in ice-cold oxygenated (95% O₂/5% CO₂) cutting solution (containing [in mM] 87 NaCl, 37.5 choline chloride, 25 NaHCO₃, 25 glucose, 2.5 KCl, 1.25 NaH₂PO₄, 7 MgCl₂, and 0.5 CaCl₂). Hippocampal coronal slices (270 μm thick) were then cut on a vibratome (VT1200S; Leica, Wetzlar, Germany). The slice was incubated in the oxygenated cutting solution for 25 minutes at 30°C and then transferred into oxygenated saline (containing [in mM] 125 NaCl, 26 NaHCO₃, 25 glucose, 2.5 KCl, 1.25 NaH₂PO₄, 1 MgCl₂, and 2 CaCl₂) for 25 minutes at 30°C before electrophysiological recordings.

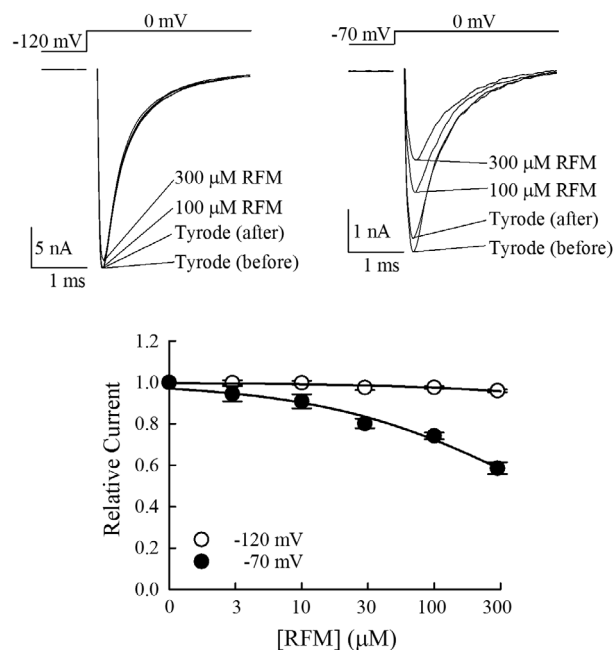


FIGURE 1: The apparent binding affinity of rufinamide (RFM) to Na⁺ channels at -70 and -120 mV. (Top) The cell was held at -120 (left) or -70 mV (right) and stepped every second to 0 mV for 3 milliseconds before (Tyrode, before) and after application of RFM (100–300 μM). The inhibitory effect of RFM is evident with a holding potential of -70 mV but not -120 mV, and the effect is reversible by washout of drugs (Tyrode, after). (Bottom) Concentration-dependent inhibition of Na⁺ currents by RFM at a holding potential of -120 mV (n = 6, 6, 5, 8, and 6, respectively) or -70 mV (n = 9, 8, 8, 17, and 9, respectively). The peak current in drug is measured when steady-state inhibition is reached (usually within seconds), and is normalized to that in control (before drug) to give the relative current. The lines are fits to each set of data and are of the following form: relative current = 1/(1 + [RFM]/K_{app}), where [RFM] is RFM concentration and K_{app} is the apparent dissociation constant of RFM, and is 242.2 and 573.7 μM at holding potentials of -120 and -70 mV, respectively.

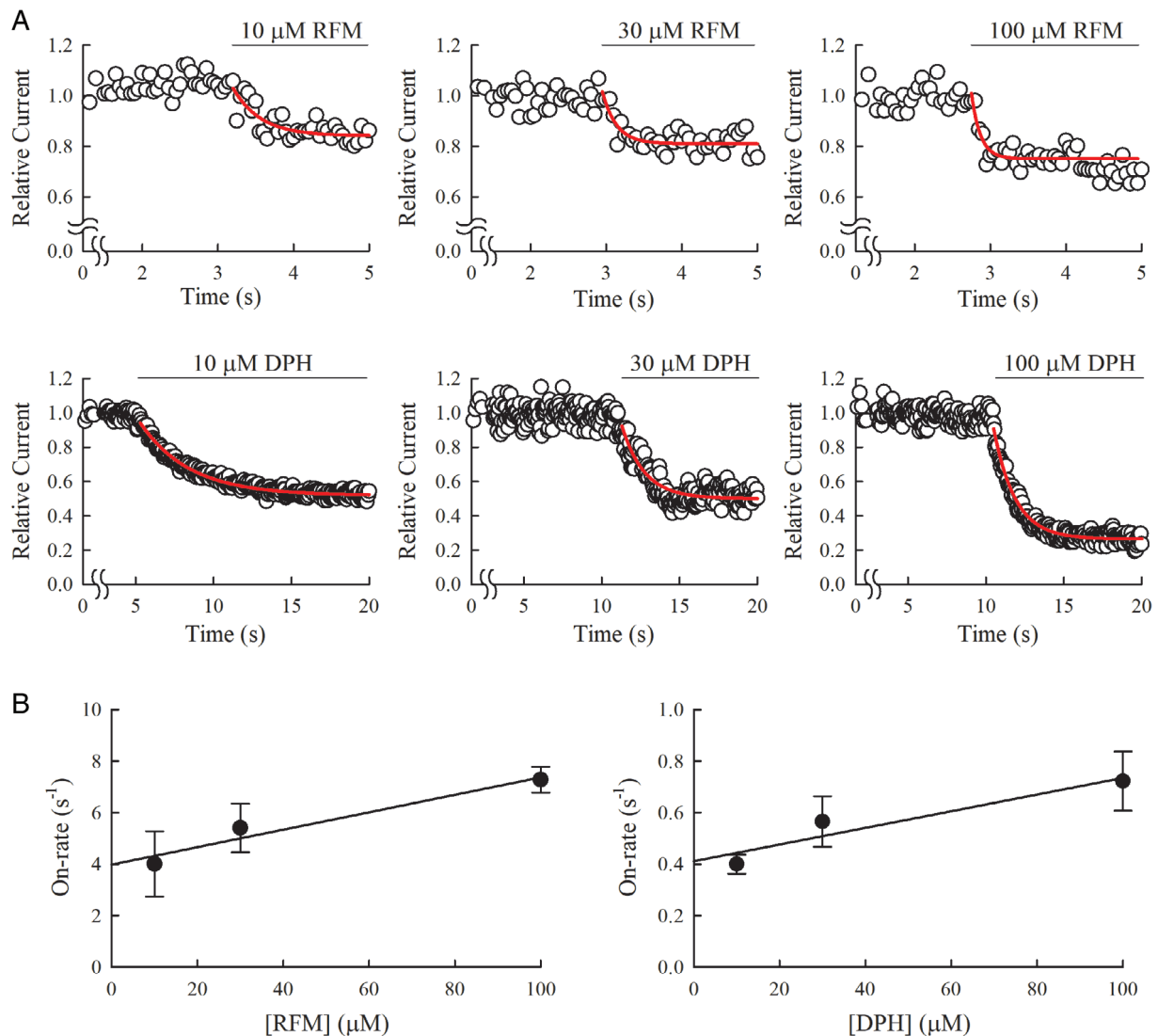


FIGURE 2: The binding kinetics of rufinamide (RFM) and phenytoin (DPH) to Na⁺ channels at -70mV . (A) The cell was held at -70mV , and stepped every 50 milliseconds to 0mV for 1 millisecond. The normalized peak current amplitude is plotted over time before and after application of different concentrations (10, 30, or $100\mu\text{M}$) of RFM (top row) or DPH (bottom row). The curves are monoexponential fits to the data points after drug application, showing higher binding rates with higher concentrations of RFM (time constants of 0.36, 0.18, and 0.12 seconds) or DPH (time constants of 3.08, 1.44, and 1.38 seconds). (B) The reciprocals of the time constants from the monoexponential fits in A are plotted against drug concentration. The line is the best linear regression fit to the data points with the slope and y-intercept of $3.4 \times 10^4 \text{ M}^{-1} \text{ s}^{-1}$ and 4.0 s^{-1} for RFM (left, $n = 5, 8, \text{ and } 8$ for 10, 30, and $100\mu\text{M}$, respectively), and $3.2 \times 10^3 \text{ M}^{-1} \text{ s}^{-1}$ and 0.41 s^{-1} for DPH (right, $n = 5, 5, \text{ and } 4$ for 10, 30, and $100\mu\text{M}$ respectively), respectively. [Color figure can be viewed at www.annalsofneurology.org]

Electrophysiological Recording in Brain Slices

An acute hippocampal slice was brought to a recording chamber with oxygenated saline stably infused by a peristaltic pump (Gilson, Middleton, WI) at a rate of $\sim 5\text{ml}/\text{min}$. Hippocampal CA1 pyramidal neurons were visualized with a $\times 60$ water immersion objective on an upright microscope (BX51WI; Olympus, Tokyo, Japan). The neurons were then recorded in whole-cell current-clamp modes at room temperature with pipettes filled with K⁺-based solution (in mM, 116 KMeSO₄, 6 KCl, 2 NaCl, 20 hydroxyethylpiperazine ethane sulfonic acid [HEPES], 0.5 ethyleneglycoltetraacetic acid [EGTA], 4 MgATP, 0.3 NaGTP, and 10 NaPO₄ creatine, pH 7.25 adjusted with KOH) and having a resistance of 3 to

$6\text{M}\Omega$. The electrodes were made from borosilicate capillaries (Harvard Apparatus, Holliston, MA; 1.65mm outer diameter, 1.28mm inner diameter) and by a micropipette puller (DMZ-ZeitZ-Puller; ZeitZ-Instruments, Martinsried, Germany). In Figure 6, burst discharges were elicited by intracellular injection of 5 consecutive 200-millisecond step currents with 1-second intervals between steps. The amplitude of the injected current was adjusted for each neuron to be the minimum that reliably evokes 5 spikes in the first step, and was generally 100 to 150pA with a baseline membrane potential of -80mV and 50 to 80pA with a baseline membrane potential of -60mV , yielding a rather constant plateau potential at -50 to -55mV for both cases. We chose -80 and -60mV as the

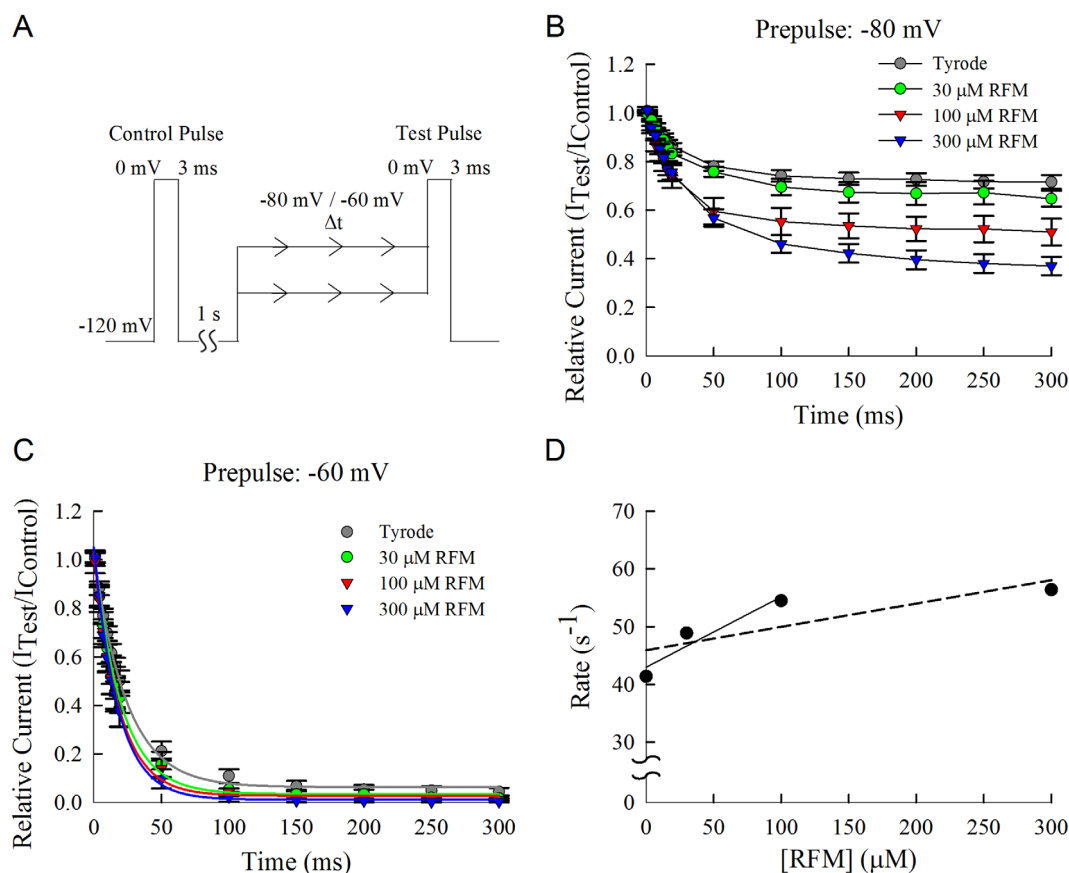


FIGURE 3: The stronger inhibitory effect of rufinamide (RFM) at -60 than at -80 mV. (A–C) The cell was held at -120 mV, and stepped to a test pulse 0 mV for 3 milliseconds to get the control current (I_{Control}). The cell was then held at -120 mV for 1 second and stepped to an inactivating pulse at -80 mV (B) or -60 mV (C) for different lengths ($1, 4, 7, 10, 13, 16, 19, 50, 100, 150, 200, 250,$ and 300 milliseconds). The second test pulse of 0 mV was then applied to obtain the residual current (I_{Test}), which was normalized to I_{Control} and plotted against the inactivating time. The time courses of decrease of currents with an inactivating pulse at -80 mV could not be reasonably fitted with monoexponential functions, and thus the lines connecting the data points are drawn by hand. The time to 50% decay in current amplitude is $34, 19, 31,$ and 31 milliseconds in the absence ($n = 16$) and presence of $30, 100,$ and $300 \mu\text{M}$ RFM ($n = 4, 7, 8$), respectively (B). The time courses of decrease of currents with an inactivating pulse at -60 mV, however, are well fitted with monoexponential functions in the absence ($n = 9$) and presence of $30, 100,$ and $300 \mu\text{M}$ RFM ($n = 4, 5,$ and 4), with time constants of $24.2, 20.5, 18.3,$ and 17.7 milliseconds, respectively (C). (D) The inverses of the time constants in C are plotted against RFM concentrations. The solid line is a linear regression fit to the data points in control (Tyrode), $30 \mu\text{M}$ RFM, and $100 \mu\text{M}$ RFM with a slope and y-intercept of $1.2 \times 10^5 \text{ M}^{-1} \text{ s}^{-1}$ and 43.0 s^{-1} , respectively. The dashed line is a linear regression fit to all 4 data points in control and $30, 100,$ and $300 \mu\text{M}$ RFM with a slope and y-intercept of $4.0 \times 10^4 \text{ M}^{-1} \text{ s}^{-1}$ and 46.0 s^{-1} , respectively. Note the apparent deviation of the data point in $300 \mu\text{M}$ RFM from the linearity set by the data points in control, $30 \mu\text{M}$ RFM, and $100 \mu\text{M}$ RFM. [Color figure can be viewed at www.annalsofneurology.org]

baseline membrane potential here based on the findings in Figures 3–5, where the effect of rufinamide is much smaller, with a prepulse of -80 mV rather than -60 mV. Recordings were acquired with a Multiclamp 700B amplifier (MDS Analytical Technologies, Sunnyvale, CA), filtered at 1 kHz, and digitized at 10 to 20 kHz with a Digidata-1440 analog/digital interface (MDS Analytical Technologies).

Electrophysiological Recording in Acutely Dissociated Hippocampal Neurons

For preparation of acutely dissociated hippocampal neurons, we first obtained brain slices from C57/BL6 mice of both sexes and aged $p7$ to $p14$ with procedures similar to those described above, except that $400 \mu\text{m}$ -thick slices were cut for this purpose. The

CA1 region was dissected from the slices and cut into small chunks. After treatment for 5 to 10 minutes at 37°C in dissociation medium (in mM, $82 \text{ Na}_2\text{SO}_4, 30 \text{ K}_2\text{SO}_4, 3 \text{ MgCl}_2,$ and 10 HEPES , $\text{pH} = 7.4$) containing 0.25% trypsin-ethylenediaminetetraacetic acid (EDTA; $1\times$; Gibco, Waltham, MA), tissue chunks were moved to dissociation medium containing no trypsin but 1 mg/ml bovine serum albumin (Sigma-Aldrich, St Louis, MO). Each time when cells were needed, 2 to 3 chunks were picked and triturated to release single neurons. The dissociated neurons were put in a recording chamber containing Tyrode solution (in mM, $150 \text{ NaCl}, 4 \text{ KCl}, 2 \text{ MgCl}_2, 2 \text{ CaCl}_2,$ and 10 HEPES , $\text{pH} = 7.4$). Whole-cell voltage clamp recordings were obtained using pipettes pulled from borosilicate micropipettes (outer diameter = 1.55 – 1.60 mm ; Hilgenberg,

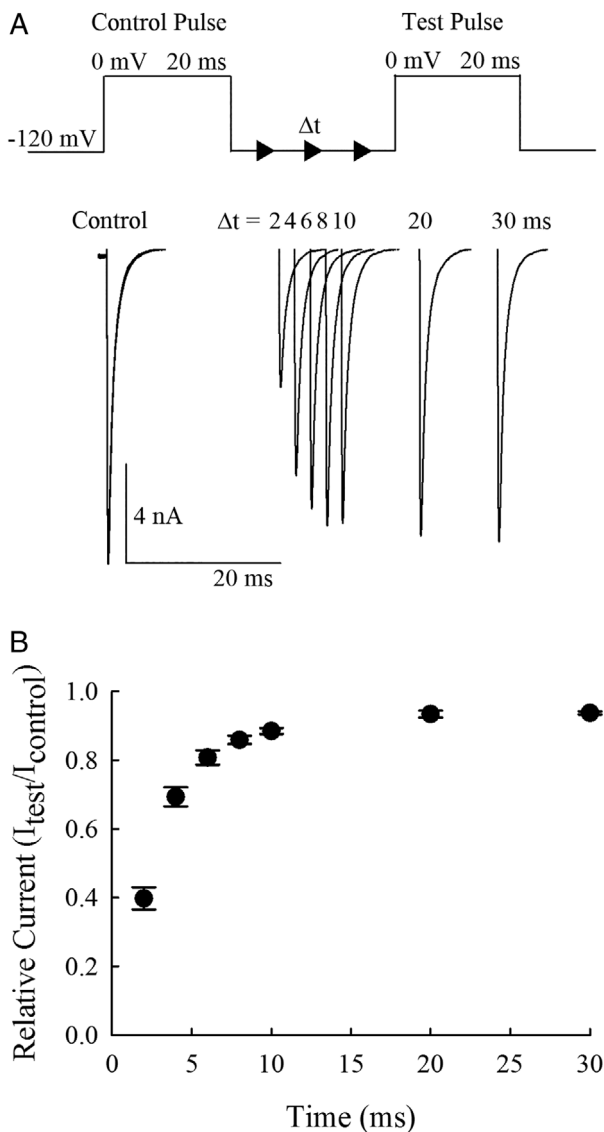


FIGURE 4: The recovery course from fast inactivation. (A) The cell was held at -120mV , and stepped to 2 consecutive pulses at 0mV for 20 milliseconds with an intervening gap at -120mV of 2, 4, 6, 8, 10, 20, or 30 milliseconds. The currents at the first and second 0mV pulses are shown, with the length of the -120mV gap indicated above each current. (B) The relative current is derived by normalization of the current in the second pulse to that in the first pulse of every sweep, and is plotted against the length of the intervening gap to obtain the time course of recovery from fast inactivation ($n = 6$).

Malsfeld, Germany), fire polished, and filled with the standard internal solution containing (in mM) 75 CsCl, 75 CsF, 3 MgCl_2 , 10 HEPES, and 5 EGTA, pH adjusted to 7.4 by CsOH. Seal was formed and the whole-cell configuration obtained in Tyrode solution. The cell was then lifted from the bottom of the chamber and moved in front of an array of flow pipes (Microcapillary; Drummond Scientific Company, Broomall, PA; content = $1\mu\text{l}$, length = 64mm) emitting external recording solutions, which were Tyrode solution with or without different concentrations of drugs. Currents were recorded at room temperature (-25°C)

with an Axopatch 200A amplifier, filtered at 5kHz with a 4-pole Bessel filter, digitized at 40-microsecond intervals, and stored using a Digidata-1322A analog/digital interface along with pCLAMP software (Molecular Devices, Sunnyvale, CA). Series resistance was generally between 1 and $3\text{M}\Omega$. The pulse protocols are detailed in each figure. The interpulse interval was in general 1 to 4 seconds, which was repeatedly checked to assure full recovery of the inactivated channel back to the baseline or resting state.

AY-9944 Model and Behavioral Tests

An acute AY-9944 mouse model was established by daily subcutaneous injection of AY-9944 (7.5mg/kg ; Tocris Bioscience, Bristol, UK) into C57/BL6 mice of both sexes from p3 to p6 according to the literature.²⁴ In some groups of mice, 50mg/kg rufinamide or 40mg/kg phenytoin was always coinjected with AY-9944. Behavioral tests were performed at p7. Despite no apparent seizure behaviors being observed, the mice receiving AY-9944 injection showed delayed response to postural changes. The mice were put upside down manually every 30 seconds, and the time for tuning over from the upside-down body posture was evaluated in a 5-minute session. After behavioral tests, acute brain slices were obtained for electrophysiological recording. The chronic AY-9944 mouse model was also established by consecutive subcutaneous injection of AY-9944 (7.5mg/kg , Tocris Bioscience) into C57/BL6 mice of both sexes on p2, p8, p14, and p20 according to the literature.^{25–27} In vivo electrophysiological recordings and behavioral tests were then performed on p45 to p50.

PTZ Model and Behavioral Tests

C57BL/6 mice (p30–p40 and 11–21g) were pretreated with vehicle (75% dimethylsulfoxide [DMSO] and 0.25% methylcellulose in ddH_2O) or anticonvulsant drugs (50mg/kg rufinamide or 40mg/kg phenytoin in vehicle) before injection of 40mg/kg PTZ (in 0.9% NaCl); all treatments were given intraperitoneally.^{28,29} The behavioral tests were performed 5 minutes after drug injection. When the animal had showed no gross movement for >10 seconds, the whiskers and ears on each side were touched twice with a cotton swab within 3 seconds, and the responsiveness (presence or absence of response) was documented. The 3-second trials were repeated every 10 seconds for a total period of 8 minutes, or would be stopped prematurely when the animal started to move or have high-stage seizures (Racine stage 3 or above). The difference between the normalized numbers of trials with no response (normalized to the total test time) before and after PTZ injection is defined as the absence index. After the behavioral tests, acute brain slices were obtained for electrophysiological recordings.

Animals and Stereotaxic Surgery

Three- to 5-week-old normal mice and 5- to 6-week-old AY-9944-treated mice were anesthetized by intraperitoneal injection of 1ml/kg of a saline mixture solution containing 50mg/ml Zoletil 50 (Virbac, Carros, France) and xylazine (Sigma-Aldrich)

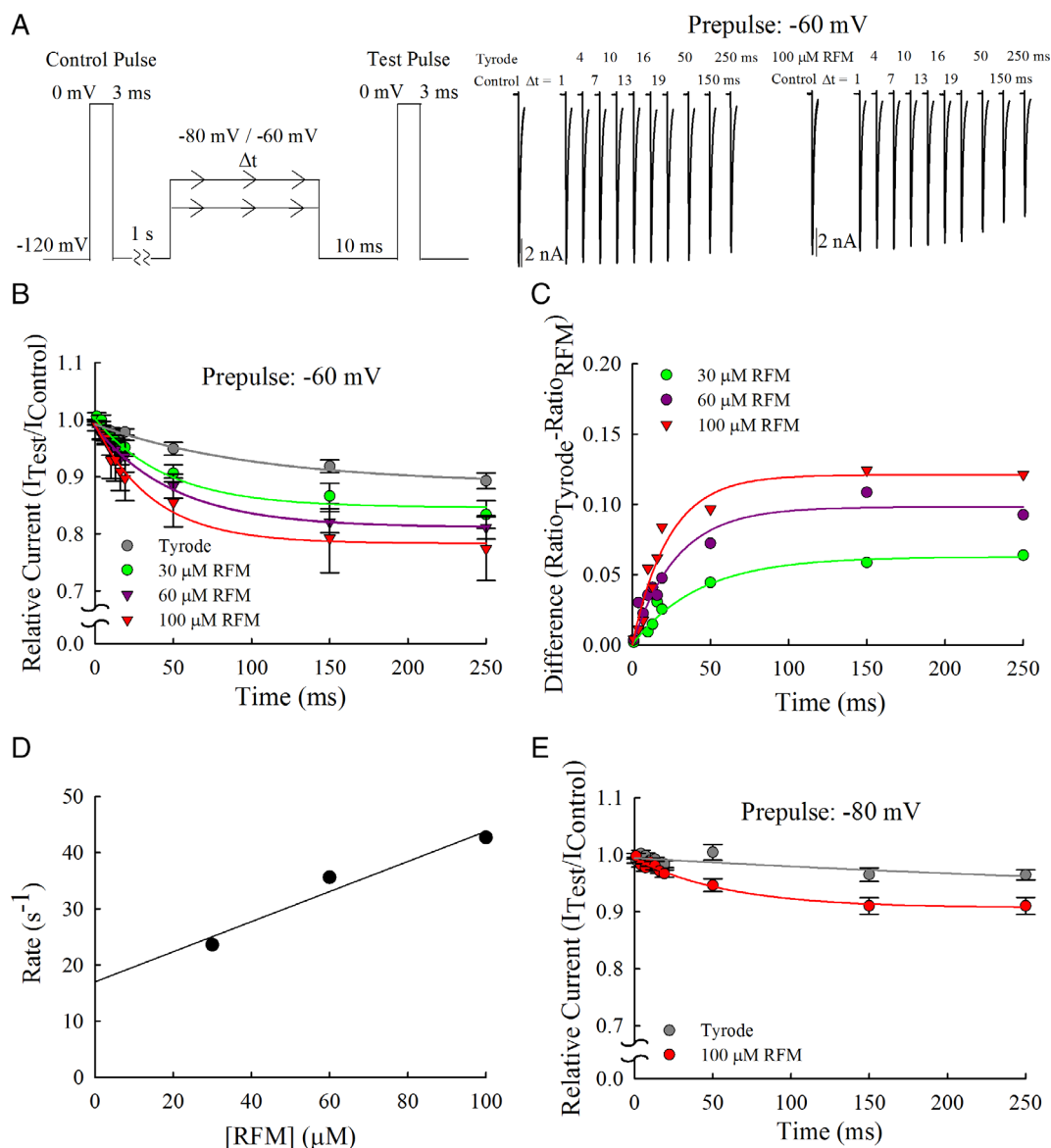


FIGURE 5: The binding kinetics of rufinamide (RFM) onto the inactivated channel at -60 mV. (A) The cell was held at -120 mV, and stepped to a first test pulse of 0 mV for 3 milliseconds to get the control current. The cell was then held at -120 mV for 1 second and stepped to an inactivating pulse at -60 mV (or -80 mV in E) for different lengths (1, 4, 7, 10, 13, 16, 19, 50, 150, or 250 milliseconds). The second test pulse of 0 mV was then applied after an intervening gap at -120 mV for 10 milliseconds to recover most drug-free fast inactivated channels. The representative currents in the absence (Tyrode) and presence of $100 \mu\text{M}$ RFM from the same neuron are overlaid according to the time sequence of examination. The length of the intervening gap is indicated above each current. (B) The relative current is derived by normalization of the current in the second test pulse to that in the first test pulse of every sweep, and is plotted against the length of the inactivating pulse at -60 mV. The lines are best fits with monoexponential functions with time constant of 104, 50, 50, and 33 milliseconds in the absence and presence of 30– $100 \mu\text{M}$ RFM ($n = 17, 8, 6,$ and $5,$ respectively). (C) The difference between the mean values in control (Tyrode) and in RFM in B is replotted against the length of the inactivating pulse. The lines are fits with monoexponential functions and time constant of 42.7, 28.1, and 23.4 milliseconds for 30, 60, and $100 \mu\text{M}$ RFM, respectively. (D) The inverse of the time constant in C is plotted against RFM concentration. The line is a linear regression fit to the data points with a slope and y-intercept of $2.7 \times 10^5 \text{ M}^{-1} \text{ s}^{-1}$ and 17.0 s^{-1} , respectively. (E) The same plot as that in B, except that the inactivating pulse is set to -80 mV. The lines are best fits of monoexponential functions with time constant of 500 and 50 milliseconds in the absence and presence of $100 \mu\text{M}$ RFM, respectively (each $n = 6$). [Color figure can be viewed at www.annalsofneurology.org]

and were placed on a stereotaxic frame (David Kopf Instruments, Tujunga, CA). Six parallel tungsten electrodes 0.16 mm apart from each other (0.0015 inches in diameter; California Fine Wire Co, Grover Beach, CA) were implanted into the primary motor cortex (anterior 1 mm, lateral 1–2 mm, and depth

0.16–1 mm from the bregma) for local field potential (LFP) recordings. Two screws bundled with silver wires were locked on the nasal bone and the skull over the cerebellum for ground and reference signals. After surgery, mice were allowed to recover for at least 7 days before in vivo electrophysiological recordings.

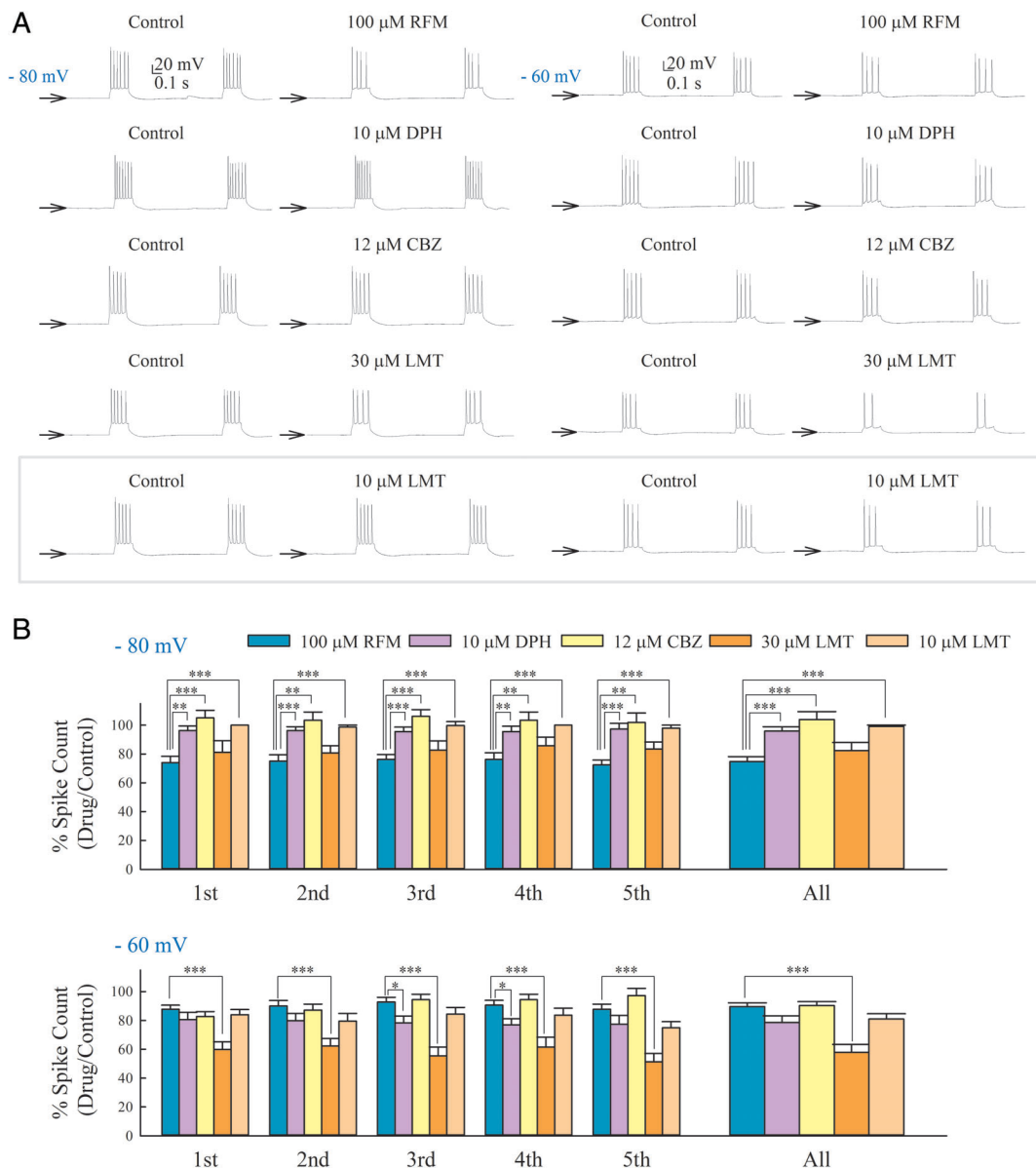


FIGURE 6: The stronger inhibitory effect of rufinamide (RFM) than phenytoin (DPH), carbamazepine (CBZ), and lamotrigine (LMT) on short burst discharges with hyperpolarized interburst intervals. (A) Short burst discharges with a plateau of -50 to -55 mV were elicited by 5 consecutive 200-millisecond constant step currents (interstep interval = 1 second) in a hippocampal neuron, where the baseline membrane potential was set at either -80 (left) or -60 mV (right). Raw sweeps elicited by the first 2 current steps are shown. (B) The spike number in each of the 5 consecutive bursts (first to fifth) and the total spike number in the 5 bursts (“All”) in each drug is normalized to that in control (without drug) to give the % Spike Count. One hundred micromolars RFM ($n = 9$) and 30μ M LMT ($n = 10$), but not 10μ M DPH ($n = 12$), 12μ M CBZ ($n = 9$), and 10μ M LMT ($n = 11$), significantly decrease the spikes in bursts when the interburst (baseline) membrane potential is -80 mV. On the other hand, most of the drugs decrease the spikes in bursts with an interburst potential of -60 mV, where 100μ M RFM seems to have the least prominent effect. * $p < 0.05$, ** $p < 0.01$, *** $p < 0.001$ compared to the RFM group by Mann-Whitney U test. [Color figure can be viewed at www.annalsofneurology.org]

In Vivo Electrophysiological Recordings and Analysis

In vivo electrophysiological signals were recorded via an amplifier (Model 3600; A-M Systems, Sequim, WA), band-pass filtered (0.3–3 kHz), amplified 1,400 times, and digitized/sampled at 25 kHz by an analog-to-digital converter (DataWave Technologies, Loveland, CO). PTZ was dissolved in normal saline. Rufinamide and phenytoin were dissolved in 75% DMSO and

0.25% methylcellulose in ddH₂O for injection. Animals were placed into the observation box for 10-minute baseline recordings. A single dose of PTZ (40 mg/kg) was then administered intraperitoneally for the control experiment. On the second day, rufinamide (50 mg/kg) or phenytoin (40 mg/kg) followed by PTZ (40 mg/kg) in 15 minutes was applied after baseline recordings to investigate the drug effect. Behavioral and electrophysiological changes were observed for 1 hour following PTZ administration.

Behavioral scores were evaluated with modified Racine stages: stage 0, normal behavior; 0.5, behavioral arrest, absencelike behavior; 1, facial and mouth clonus; 2, head nodding; 3, unilateral forelimb clonus; 4, bilateral forelimb clonus with rearing; 5, rearing and falling; 6, wild running and jumping; 7, tonic

posturing. In AY-9944-treated mice, rufinamide (50mg/kg) was injected intraperitoneally after 30-minute baseline recordings. Behavioral and electrophysiological changes were documented for another 1 hour following rufinamide administration. After rest for 24 hours, the same procedures with phenytoin

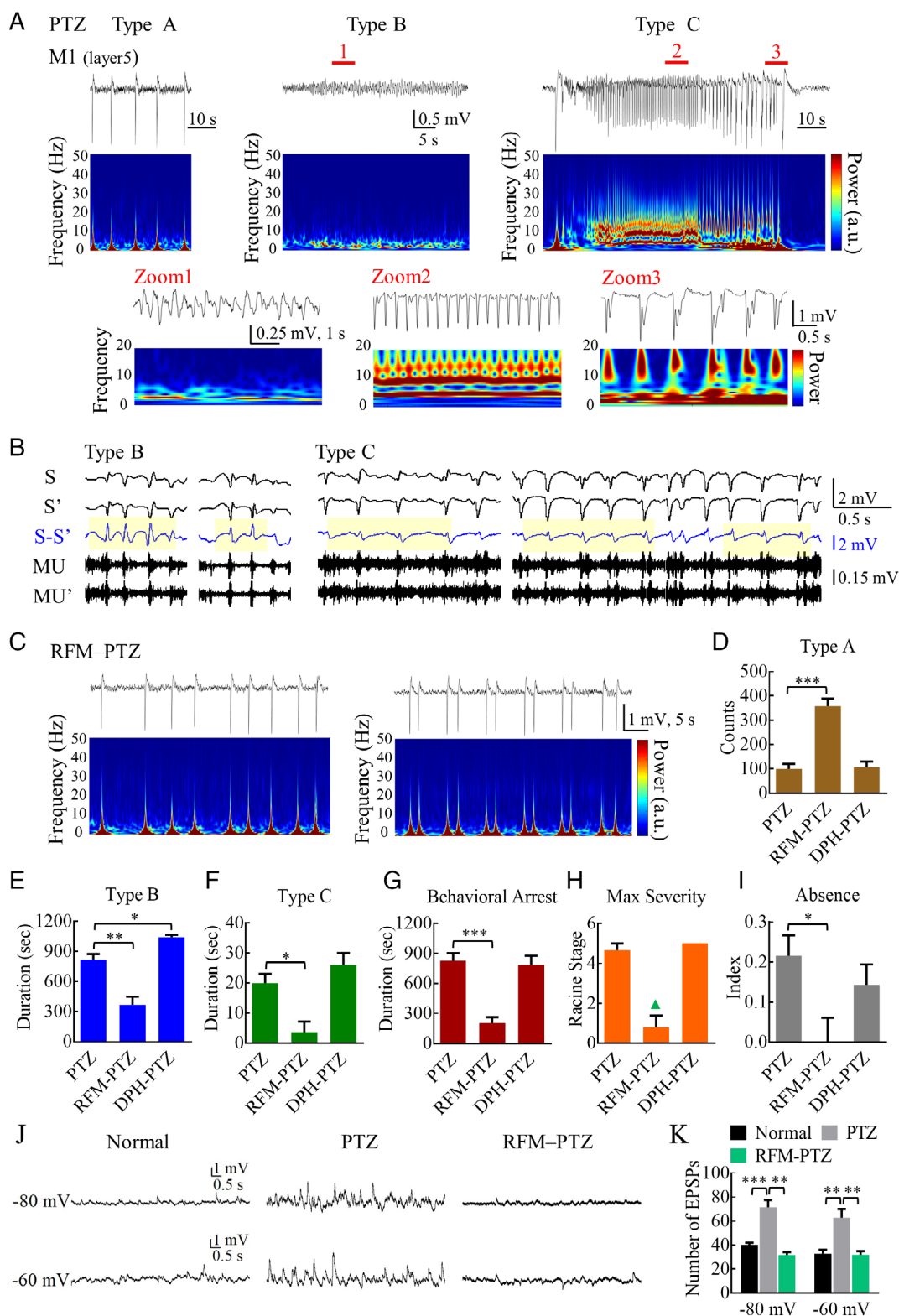


(Figure legend continues on next page.)

(40mg/kg) were repeated in the AY-9944-treated mice. For LFP recordings and multiunit recordings, signals were band-pass filtered at 0.3 to 100Hz and 300 to 3,000Hz, respectively. LFPs were downsampled to 500Hz for analysis afterward. The wavelet spectrogram of LFPs was calculated from a custom-written script in MATLAB (MathWorks, Natick, MA). The power spectrum was calculated by fast Fourier transformation using Welch's method with the Hamming window (window length = 1,024 points with half of the data overlapped, giving a frequency resolution of 0.488Hz; pCLAMP 10).

Analyses and Statistics

All statistics are given as mean \pm standard error of mean. Electrophysiological data were analyzed with pCLAMP 10, SigmaPlot 12 (Systat Software, San Jose, CA), Excel 2013 (Microsoft, Redmond, WA), and PASW Statistics 18.0 (IBM, Armonk, NY) software. For statistical comparison, nonparametric Mann-Whitney *U* tests or Wilcoxon signed rank tests were used (PASW statistics 18.0; or Prism6, GraphPad Software, San Diego, CA). Methods for statistical comparison are also described in the figure legends, with a value of $p < 0.05$ indicating significant difference.

Materials

Rufinamide and lamotrigine were from Tocris Bioscience, and carbamazepine and phenytoin were from Sigma-Aldrich, and were dissolved in DMSO (Sigma-Aldrich) to make stock solutions. The final concentration of DMSO (0.3% or less) was not found to have significant effect on Na⁺ currents. AY-9944 and PTZ were purchased from Tocris Bioscience. Isoflurane was purchased from Piramal Critical Care (Bethlehem, PA), and 0.25% trypsin-EDTA(1X) was purchased from Gibco. Bovine serum albumin, methylcellulose, and all chemical salts used in this study were purchased from Sigma-Aldrich.

Study Approval

This study was performed in accordance with the recommendations in the Guide for the Care and Use of Laboratory Animals of the US National Institutes of Health. All experiments including the care and use of animals were approved by the institutional animal care and use committee of National Taiwan University College of Medicine and that of Chang Gung University, Taiwan. All efforts were made to minimize animal suffering.

Results

Rufinamide Selectively Binds to Inactivated Na⁺ Channel

Rufinamide shows only negligible effect on neuronal Na⁺ currents elicited from a holding potential of -120mV , but has manifest inhibitory effect on currents elicited from a more depolarized holding potential such as -70mV (Fig 1). The concentration-response curve gives a rough estimate of the apparent dissociation constant (K_{app}) of $\sim 242\text{mM}$ and $\sim 574\mu\text{M}$ for rufinamide binding to the Na⁺ channel (assuming a bimolecular interaction) at a holding potential of -120mV (where most channels occupy the resting state) and -70mV (where more channels are driven into the inactivated states), respectively. The very different K_{app} values with the two holding potentials suggest highly selective binding of rufinamide to the inactivated rather than the resting Na⁺ channels, like the cases of most other ASDs targeting Na⁺ channels. Because not all Na⁺ channels are inactivated at -70mV ,^{20–22} K_{app} at -70mV should be an averaged measure of the affinity of rufinamide to a mixture of different gating states. The true binding affinity of rufinamide to the inactivated channels (K_I) therefore should be less than $\sim 574\mu\text{M}$. Nevertheless, the estimated K_I value is quite higher than that ($\sim 17\text{--}70\mu\text{M}$) of phenytoin, carbamazepine, or lamotrigine

FIGURE 7: Inhibition of pentylenetetrazol (PTZ)-induced absencelike seizure discharges and behaviors by rufinamide (RFM) rather than phenytoin (DPH). (A) After intraperitoneal injection of PTZ, local field potential (LFP) recordings were obtained from the primary motor cortex (M1; layer 5) for 1 hour. Basically, three types (types A, B, and C) of electrophysiological seizure patterns are discernible. The lower panels show the zoomed pictures for the typical segments (marked as 1, 2, and 3 in red) of types B and C. (B) Two unipolar recordings for types B and C from 2 neighboring electrodes (S and S') are subtracted from each other (S-S') to simulate the bipolar recordings on the electroencephalogram. The spike-and-wave features (yellow area) could be more manifest in bipolar recordings (although not necessarily). Also note that the concomitant multiunit (MU) activities are grouped to the spike rather than the wave phases in LFPs. (C, D) After treatment with RFM, type A discharges tend to persist in the PTZ model, and could even be increased in a 30-minute period after PTZ. (E, F) Type B and C discharges are markedly decreased (type B) or essentially abolished (type C) in the presence of RFM but essentially unaffected by DPH. (G, H) Behaviorally, the total duration of behavioral arrest (G) as well as the maximal Racine stage ever reached (H) in a 30-minute period after PTZ is markedly decreased by RFM but not DPH. The green triangle is a reminder that in the presence of RFM, myoclonic jerks may persist or are even increased with Racine stage 0. For D through H, $n = 5$ and 4 for the RFM and DPH groups, respectively. (I) The absence index is calculated according to mouse responsiveness to whisker and ear touching after PTZ injection. RFM ($n = 12$) rather than DPH ($n = 4$), if compared to vehicle (PTZ, $n = 15$), markedly decreases the absence index. (J, K) Acute brain slices were obtained after the behavioral experiments in I. There are significantly increased spontaneous excitatory postsynaptic potentials (EPSPs) in hippocampal neurons from PTZ-injected mice (baseline potential of -80mV , $n = 8$; -60mV , $n = 8$) compared to normal mice (-80mV , $n = 7$; -60mV , $n = 6$) or mice injected with both PTZ and RFM (-80mV , $n = 5$; -60mV , $n = 4$). The number of EPSPs refers to the total count in a 30-second period of continuous recording. * $p < 0.05$, ** $p < 0.01$, *** $p < 0.001$, Mann-Whitney *U* test. See Materials and Methods for details and drug dosages.

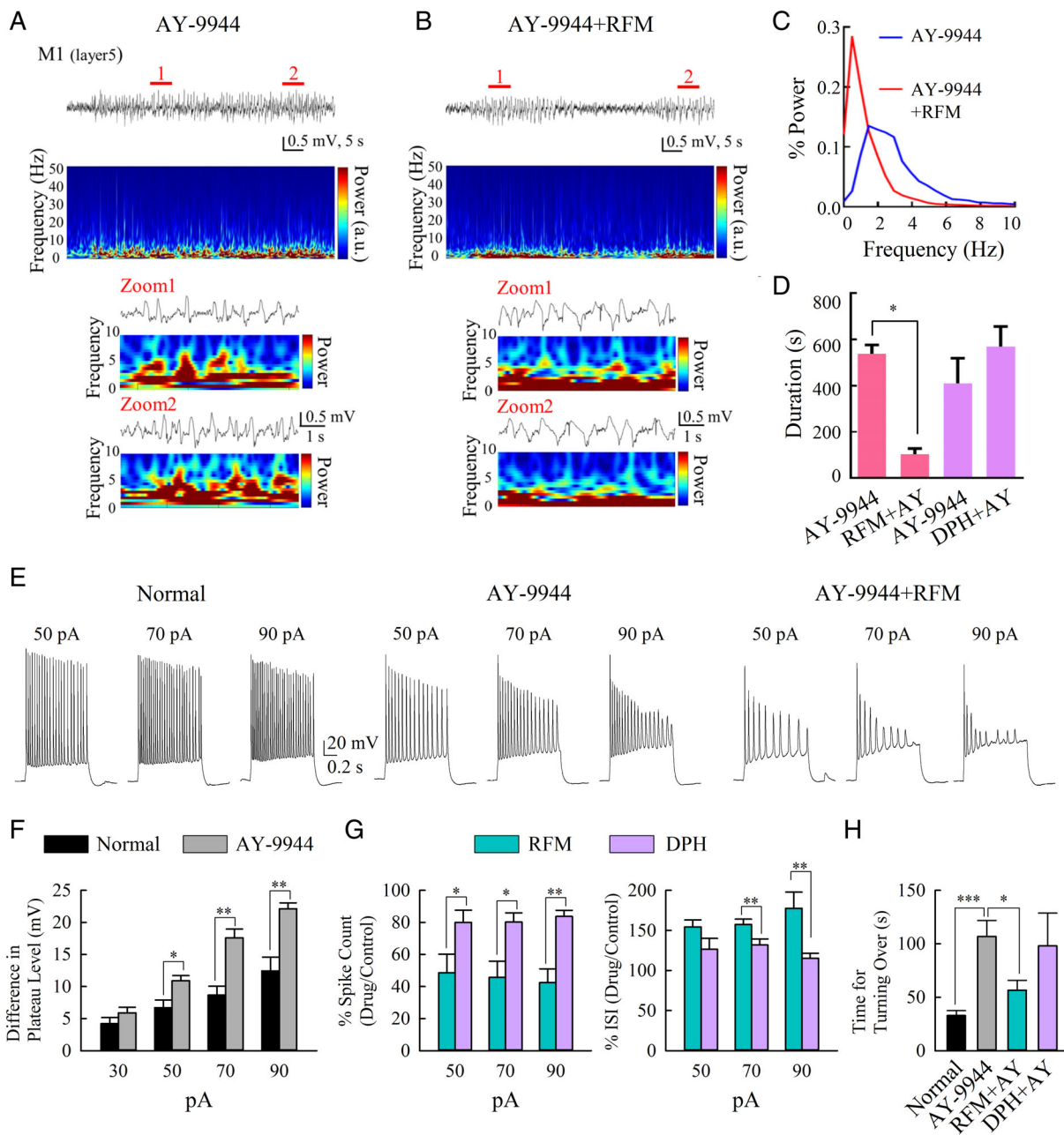


FIGURE 8: Amelioration of the electrophysiological and behavioral changes in the AY-9944 model by rufinamide (RFM) rather than phenytoin (DPH). (A) In the chronic AY-9944 model, spike and wave discharges (SWDs) are discernible in the local field potential recordings in the primary motor cortex (M1; layer 5). The SWDs are similar to type C epileptiform discharges in Figure 7, repeating at a frequency of 2 to 7 Hz (see concomitant wavelet spectrograms shown below the raw sweeps), but with much smaller amplitude. The indicated segments (marked as 1 and 2 in red) are zoomed in the lower panels. (B) In the presence of RFM, the SWDs regress into slow waves at 0.5 to 2 Hz, or even disappear. Note the prominent shift of the major frequency of oscillation to a lower range in the concomitant wavelet spectrograms displayed below the raw sweeps. (C) The power spectrums of the sweeps in A and B (ie, before and after RFM, respectively) show a clear shift to the left (lower frequencies) by RFM. (D) The total duration of SWDs in a 30-minute period (ie, 15–45 minutes after the introduction of drugs) is markedly shorter in the case of RFM ($n = 6$) but not DPH ($n = 6$). $*p < 0.05$, Wilcoxon signed rank test. (E–G) In the acute AY-9944 model ($n = 5$), the membrane potential plateau level (see F) and thus the depolarization block phenomenon in response to step current injection (30–90 pA) are more prominent if compared to that in normal mice ($n = 5$). The difference in plateau level is defined as the difference between the lowest potentials between the first and the last 2 spikes on the plateau. The spike counts and the interspike intervals (ISIs) of the first 3 spikes in response to step current injection are much more decreased and increased, respectively, with coinjection of RFM ($n = 6$) than DPH ($n = 4$). (H) Mice of the acute AY-9944 model ($n = 14$) show significantly delayed response to postural changes and thus increased time for tuning over from the upside-down body posture if compared to normal mice ($n = 9$). The delay is markedly shortened if AY-9944 is coinjected with RFM ($n = 6$) but not DPH ($n = 5$). $*p < 0.05$, $**p < 0.01$, $***p < 0.001$, Mann–Whitney U test. See Materials and Methods for details and drug dosages.

measured in a similar condition.^{20–22} The superiority of rufinamide to phenytoin in the treatment of LGS thus is unlikely to be ascribable to a higher affinity toward the inactivated Na⁺ channels.

Rufinamide Has Faster Binding Kinetics Than Classical Na⁺ Channel Inhibitors

We then investigated the binding rate of rufinamide. Neuronal Na⁺ currents were consecutively elicited by a 3-millisecond test pulse from a holding potential of -70mV every 50 milliseconds. The test pulse was deliberately given so often as to increase the resolution of the kinetics. In the meanwhile, the test pulse was deliberately made short to avoid any cumulative effect of the repetitive depolarization. Consistent with a bimolecular reaction, rufinamide reduces the elicited currents with monoexponential kinetics and the macroscopic binding rates are linearly correlated with rufinamide concentration, giving a slope or a macroscopic binding rate constant of $\sim 3.4 \times 10^4 \text{ M}^{-1} \text{ s}^{-1}$, and a y-intercept or an unbinding rate of $\sim 4.0 \text{ s}^{-1}$ at -70mV (Fig 2). These rates are much faster than that of phenytoin measured in the same condition ($\sim 3.2 \times 10^3 \text{ M}^{-1} \text{ s}^{-1}$ and $\sim 0.41 \text{ s}^{-1}$ at -70mV , respectively). It should be noted that the true binding rates shall be even faster, as not all of the channels are inactivated at -70mV . The ratio between the unbinding rate and the macroscopic binding rate constant gives a rough estimate of the dissociation constant of $\sim 118\mu\text{M}$ for rufinamide at -70mV based on a bimolecular reaction. This is consistent with the idea that the estimate from the steady-state inhibition data in Figure 1 ($\sim 574\mu\text{M}$) could be an underestimate. Because rufinamide seems to be quantitatively distinct from the other Na⁺ channel inhibitors in terms of the kinetics of action, it is desirable to have further measurements on the binding rates with more channels kept in the inactivated state. However, it is difficult to directly measure the kinetics at -60mV or more depolarized membrane potentials with a method similar to that in Figure 2. If most channels are driven into the inactivated states, the currents would be too small to be accurately recorded. We therefore had a different approach with gradually lengthened depolarizing pulses at -60 versus -80mV (Fig 3). Rufinamide evidently has a stronger effect at -60mV than -80mV . Also, the time courses of decrease of current could not be described by monoexponential functions with an inactivating pulse of -80mV , and are apparently not rufinamide dose-dependent (the time for 50% decay does not change monotonously with the concentration of rufinamide). In contrast, the time courses of decrease of current could be described by monoexponential functions with an inactivating pulse of -60mV , and show faster decay with

higher concentrations of rufinamide. Linear regression fit to the speed of current decay at -60mV at different concentrations of rufinamide gives binding rates of $\sim 4 \times 10^4$ to $1.2 \times 10^5 \text{ M}^{-1} \text{ s}^{-1}$ (see Fig 3D). The wide range of variation is at least partly ascribable to the already very fast current decay even in the control condition. The apparent deviation from linearity of the data point in $300\mu\text{M}$ rufinamide also suggests that the macroscopic binding rate at such a high concentration has approached the speed of gating (generation of the corresponding inactivated states), and the binding step therefore is not so “rate-limiting” in the whole process of rufinamide action.

Rufinamide Binds to Inactivated Na⁺ Channel with Ultrafast Rate of $\sim 2.7 \times 10^5 \text{ M}^{-1} \text{ s}^{-1}$

In view of the probable uniqueness of binding kinetics of rufinamide, we had yet another approach to have a more accurate measurement. The time course of recovery from inactivation shows that most of the inactivated Na⁺ channel shall recover within ~ 10 milliseconds at -120mV in control conditions (Fig 4). It is then plausible that, in the presence of rufinamide, most of the channels not recovered by the 10-millisecond gap pulse (the “nonavailable” channels) are rufinamide-bound. We therefore modified the protocols in Figure 3 with the addition of a 10-millisecond gap to -120mV , and limited the concentration of rufinamide to $\leq 100\mu\text{M}$ to avoid the probable confounding factors from high concentrations (Fig 5). With an inactivating pulse of -60mV , rufinamide decreases the available channels after the 10-millisecond gap in a dose-dependent manner. The time course of increase of nonavailable channels is also dependent on rufinamide concentration. The kinetics of generation of nonavailable channels are linearly correlated with rufinamide concentration, giving a rate constant of $\sim 2.7 \times 10^5 \text{ M}^{-1} \text{ s}^{-1}$ at -60mV . In comparison, the effect of rufinamide is much smaller with an inactivating pulse of -80mV , where $100\mu\text{M}$ rufinamide has only a slight effect to decrease the relative current by $<10\%$. A binding rate constant of $\sim 2.7 \times 10^5 \text{ M}^{-1} \text{ s}^{-1}$ is much faster than phenytoin, carbamazepine, and lamotrigine.^{20–22} Rufinamide is thus distinct among the Na⁺ channel inhibitors for the ultrafast binding rate to the inactivated Na⁺ channels.

Rufinamide Is Distinctively Effective against Short Burst Discharges with More Hyperpolarized Interburst Intervals

Seizures are typically reverberant cycles of “burst” and “suppression” phases of neuronal activities. Most classical use-dependent anticonvulsants (such as phenytoin) acting on Na⁺ channels require sufficiently long membrane

depolarization to ensure adequate binding as they selectively but slowly bind to the fast inactivated state. In contrast, we found that rufinamide binds to the inactivated channel with much faster kinetics. To demonstrate the differential effect on seizure discharges between phenytoin and rufinamide, repetitive short (~200 milliseconds) burst discharges with a plateau at -50 to -55 mV of CA1 pyramidal neurons in acute hippocampal slices were evoked with a 1-second interburst interval set at either -80 mV or -60 mV (Fig 6). The effect of $100\mu\text{M}$ rufinamide, $10\mu\text{M}$ phenytoin, $12\mu\text{M}$ carbamazepine, and $30\mu\text{M}$ lamotrigine, roughly the highest free therapeutic concentration for each drug,^{30–37} was documented. Because of its very wide therapeutic range (3 – $30\mu\text{M}$) and the scattered reports of its efficacy against seizures in LGS,^{38,39} we also tested the effect of lamotrigine at medium concentrations ($\sim 10\mu\text{M}$). Consistent with the biophysical reasoning based on the binding kinetics, rufinamide and $30\mu\text{M}$ lamotrigine, but not phenytoin, carbamazepine, or $10\mu\text{M}$ lamotrigine, significantly inhibit the short burst discharges with the interburst intervals set at -80 mV (see Fig 6). On the other hand, all drugs show an inhibitory effect on the evoked burst discharges with the interburst intervals set at -60 mV, in which case phenytoin even shows a tendency toward stronger inhibition than rufinamide. With its ultrafast binding kinetics, rufinamide may have a stronger effect on repetitive short bursts with relatively hyperpolarized interburst intervals reminiscent of the case of LGS. On the other hand, rufinamide is not completely superior to phenytoin. For short bursts with more depolarized interburst intervals (eg, -60 mV), $100\mu\text{M}$ rufinamide seems to have a smaller suppressive effect because of the lower affinity (see Fig 1) and thus weaker steady-state inhibition than $10\mu\text{M}$ phenytoin.

Rufinamide Is Distinctively Effective against SWDs In Vivo

We then investigated the effect of rufinamide in vivo in animal models with epileptiform SWDs mimicking absence or atypical absence seizures (eg, seizures in LGS). In the PTZ model, we identified 3 basic types of seizure discharges (Fig 7). Type A refers to very short isolated spikes (~ 20 – 80 milliseconds in duration). The animal could have myoclonic jerks corresponding to the spikes, but the behavior is otherwise normal during this period (Racine stage 0). Type B is characterized by repetitive spikes intermixed with waves in either unipolar or bipolar recordings, and the animals in general show absencelike behavior (“behavioral arrest,” Racine stage 0.5). It is also of note that in the concomitant multiunit recordings, the multiunit activities are grouped to the spike rather than the wave phases in LFPs. This is consistent with the classic

view that the spike and wave in SWDs are correlated to the burst and suppression periods of cellular activities, respectively. Type C is apparently an advanced form of type B, and is characterized by oscillations of larger amplitude (>4 standard deviations of baseline noise) and higher frequency (2 – 7 Hz). Behaviorally, the animal would be in Racine stage 1 to 5. After type C discharges, there is usually a period of marked postictal suppression, both electrophysiologically and behaviorally, for several seconds to minutes. Rufinamide (50 mg/kg, roughly corresponding to serum levels in therapeutic conditions^{40,41}) markedly decreases type B and C, but not type A discharges. Type A discharges are even increased, presumably ascribable to the “truncated” type B and type C discharges and suggestive of the ultimate ineffectiveness of rufinamide on the ultrashort bursts or depolarization. This is consistent with the clinical experiences of ineffectiveness or even aggravation of myoclonic jerks in LGS with rufinamide.⁴¹ In contrast, phenytoin (40 mg/kg, resulting in serum levels roughly corresponding to those in therapeutic conditions^{34,35}) shows no effect on type B and type C discharges. Behaviorally, the seizures associated with type B and type C are consistently decreased by rufinamide but not phenytoin. The overall absence index, which presumably indicates the level of impaired consciousness, is markedly ameliorated with rufinamide but not phenytoin. The mechanism of action of rufinamide may also involve a decrease of presynaptic neurotransmitter release because of inhibition of the excessively repetitive unprovoked excitatory postsynaptic potentials in PTZ. In the chronic AY-9944 model, which exhibits atypical absences mimicking LGS,^{25–27} rufinamide again attenuates SWDs, with a marked shift of the power spectrum of local field potentials to lower frequencies (Fig 8). In the acute AY-9944 model,²⁴ rufinamide accordingly reduces the burst discharges in slice recordings, an effect evidently stronger than phenytoin. Behaviorally, the animals also show marked improvement in responsiveness with rufinamide but not phenytoin.

Discussion

Suppression of SWDs and Seizures in LGS: Requirement and Limitation of Fast Drug Binding

The ictal discharges and network activities in LGS are partly similar to typical absence seizures and are characterized by repetitive short depolarization (burst) followed by much longer repolarization, corresponding to a spike (~ 70 milliseconds, or a slightly longer sharp wave) followed by a wave up to 350 to 400 milliseconds in length on EEG (eg, see Fig 7B).¹ The depolarization is too short for significant binding and action of the classical

slow-binding Na⁺ channel inhibitors such as phenytoin. We have seen that the binding rate constant of rufinamide to the inactivated Na⁺ channel is >~20-fold faster than phenytoin (see Fig 2). Together with the ~10-fold higher therapeutic concentrations of rufinamide in the cerebrospinal fluid,^{33–35} the macroscopic binding rate of rufinamide could be extraordinarily fast (ie, >~200-fold faster than phenytoin). Rufinamide at 100μM, roughly the highest therapeutic concentration, may therefore take on average only ~40 milliseconds to bind to the inactivated Na⁺ channel to suppress the burst discharges (eg, see Figs 6 and 8E). This is an estimate based on in vitro data at room temperatures, and the action could be faster at body temperatures. In vivo studies confirm the suppressive effect on SWDs and the concomitant amelioration of absencelike symptoms (eg, behavioral arrest) in different seizure models by rufinamide, but not by phenytoin (see Figs 7 and 8). Rufinamide therefore could be the drug of choice for repetitive short burst discharges rather than the classical Na⁺ channel inhibitors, especially for those interspersed with relatively hyperpolarized interburst intervals (eg, –80mV). This also explains the suppressive effect of 30μM (roughly the highest therapeutic concentration) but not 10μM lamotrigine on short bursts (see Fig 6) and a partial clinical effect of lamotrigine on LGS.^{38,39} These findings underscore the critical role of fast drug binding in the therapeutic effect on LGS, and probably also typical absence as well as the other seizures with similar SWDs on EEG. For instance, rufinamide is unequivocally effective in both PTZ and AY-9944 models. There are also reports of the efficacy of rufinamide on different focal seizures¹² or status epilepticus, which was characterized by regular fast activities (~21Hz) right before and after the onset of clinical tonic seizures in a subject having failed many other ASDs.¹⁴ These findings suggest a much wider antiseizure scope of a drug with ultrafast binding kinetics in clinical practice. However, it is of note that ultrashort bursts or depolarization could persist with myoclonic jerks in the presence of rufinamide. Because the bursts could be “cut shorter” by rufinamide, type B and C ictal discharges are decreased, but type A discharges (corresponding to short spikes on EEG) may increase. Although shorter bursts may have more limited spreading and better preserved consciousness, “aggravation” of certain types of seizures (eg, type A discharges on EEG or myoclonic jerks in behavioral manifestations in Fig 7) may be documented and could be more or less an inevitable result. In other words, if a clinically useful Na⁺ channel inhibitor has ultrafast binding kinetics, then its steady-state affinity should not be too high. Otherwise, inhibition of Na⁺ currents would ensue so quickly and

profoundly as to jeopardize many normal discharges and preclude clinical applications. For the development and use of the therapeutic agents targeting seizure discharges, the effect and the adverse effect should always be considered and balanced according to individualized situations.

Use of Na⁺ Channel Inhibitors: Pharmacological Considerations Correlative to EEG Patterns

Na⁺ channel inhibitors constitute the mainstream of ASDs, and have usually been deemed as one group of similar medications in the management of seizures. The markedly different efficacy between rufinamide and phenytoin (eg, see Figs 6–8), however, demonstrates that “Na⁺ channel inhibitor” is an oversimplified grouping. Most seizures involve reverberating burst discharges in the network, or in essence a burst–suppression pattern of neuronal activities, which usually results in rhythmic or semirhythmic waves or complexes on EEG.^{43–48} For the ASDs selectively binding to and stabilizing the inactivated Na⁺ channel, there are then 2 primary determinants of efficacy, namely, the length of the burst (depolarization) phase and the membrane potential (level of hyperpolarization) of the interburst phase. In this regard, SWDs are characterized by short bursts, which very quickly (eg, <100 milliseconds) elicit strongly repolarizing interburst phases to end the bursts and to recover the inactivated Na⁺ channels (see also Fig 7B).^{49–52} The repolarization is in general so strong in SWDs that a prominent slow wave could be recorded on EEG, during which period drug binding to the inactivated Na⁺ channel is essentially negligible. Rufinamide, a fast-binding ASD, is more effective than the others in this case because of higher chances of adequate binding during the short bursts. For the other epileptiform discharges on EEG, such as spikes/polyspikes, sharp waves, or fast/slow waves with different rhythmicity, the duration of the depolarization and the level of repolarization are more implicit and variable than SWDs. For example, rhythmic slow waves on EEG may consist of burst and repolarization phases in the first and second half of each wave, respectively, or the burst phase itself could be so long as to occupy most of the wave.^{53,54} Phenytoin then may be superior to rufinamide in these cases (eg, see Fig 6). Based on the differential requirements for an antiseizure effect, one may also contemplate the cellular attributes based on the therapeutic efficacy and look forward to more successful use of the Na⁺ channel inhibitors. For example, if phenytoin gives favorable but incomplete clinical responses, it is rational to add another “similar” drug such as carbamazepine. This is because quantitative measures indicate that the two drugs do not saturate the inactivated channel even at the highest therapeutic concentrations and at the steady state (~50% and ~30%

binding for phenytoin and carbamazepine, respectively^{20,22}). However, if there is no significant benefit with the addition of carbamazepine, then one may consider that the residual seizures are chiefly characterized by shorter bursts or more hyperpolarized interburst phases, and try rufinamide for the next move. In addition to rufinamide, lacosamide is another new and distinct Na⁺ channel-inhibiting ASD. Lacosamide preferentially and slowly binds to the slow inactivated state, which is different from the fast inactivated state and usually takes at least a few hundred milliseconds to develop.^{55–57} Consequently, lacosamide may require even stronger and longer cumulative depolarization for adequate drug binding. Lacosamide therefore could potentially have a narrower scope of antiseizure action, with less interference on normal bursts (especially those similar to seizure discharges, such as the repetitive rebound bursts in the cerebellar nuclear neurons triggered by the input from Purkinje neurons).⁵⁸ This may partly explain why there is less ataxia and fewer relevant adverse events associated with lacosamide in clinical settings.⁵⁹ In-depth considerations based on the molecular actions and therapeutic responses of ASDs are always advisable, and may in turn contribute to more pathophysiological understanding and a successful therapeutic regimen for each individual patient.

Acknowledgments

This work was supported by grants MOST107-2311-B-182-004 (to Y.-C.Y.), MOST108-2311-B-182-001 (to Y.-C.Y.), MOST109-2320-B-182-006 (to Y.-C.Y.), MOST106-2320-B-002-014-MY3 (to C.-C.K.), MOST106-2321-B-002-032 (to C.-C.K.), MOST107-2321-B-002-012 (to C.-C.K.), MOST108-2321-B-002-007 (to C.-C.K.), and MOST109-2326-B-002-001 (to C.-C.K.) from the Ministry of Science and Technology, Taiwan, and grants CMRPD1H0091-3 and CMRPD1K0661 (to Y.-C.Y.) from the Chang Gung Medical Foundation, Taiwan. The funders had no role in study design, data collection and analysis, decision to publish, or preparation of the manuscript.

We thank Dr J. Y.-C. Kuo for critically reading the manuscript and helpful discussion; and the Neuroscience Research Center of Chang Gung Memorial Hospital, Linkou, Taiwan.

Author Contributions

Y.-C.Y. and C.-C.K. contributed to the conception and design of the study; all authors contributed to the acquisition and/or analysis of data; Y.-C.Li., Y.-C.La., P.C., Y.-C.Y., and C.-C.K. contributed to preparing the figures;

Y.-C.Li., Y.-C.Y., and C.-C.K. contributed to drafting the text.

Potential Conflicts of Interest

Nothing to report.

References

- Arzimanoglou A, French J, Blume WT, et al. Lennox-Gastaut syndrome: a consensus approach on diagnosis, assessment, management, and trial methodology. *Lancet Neurol* 2009;8:82–93.
- Fitzgerald LF, Stone JL, Hughes JR, et al. The Lennox–Gastaut syndrome: electroencephalographic characteristics, clinical correlates, and follow-up studies. *Clin Electroencephalogr* 1992;23:180–189.
- Hancock EC, Cross JH. Treatment of Lennox-Gastaut syndrome. *Cochrane Database Syst Rev* 2013;2:CD003277.
- Montouris G, Aboumatar S, Burdette D, et al. Expert opinion: proposed diagnostic and treatment algorithms for Lennox–Gastaut syndrome in adult patients. *Epilepsy Behav* 2020;110:107146.
- Verrotti A, Striano P, Iapadre G, et al. The pharmacological management of Lennox-Gastaut syndrome and critical literature review. *Seizure* 2018;63:17–25.
- Food and Drug Administration. Dilantin® prescribing information. 2018. Available at: https://www.accessdata.fda.gov/drugsatfda_docs/label/2018/084349s0851bl.pdf. Last accessed 23 February, 2021.
- Food and Drug Administration. Tegretol® prescribing information. 2018. Available at: https://www.accessdata.fda.gov/drugsatfda_docs/label/2018/016608s115_018281_s058_018927s055_020234_s047.pdf. Last accessed 23 February, 2021.
- Striano P, McMurray R, Santamarina E, Falip M. Rufinamide for the treatment of Lennox-Gastaut syndrome: evidence from clinical trials and clinical practice. *Epileptic Disord* 2018;20:13–29.
- Thiele EA, Marsh ED, French JA, et al. Cannabidiol in patients with seizures associated with Lennox-Gastaut syndrome (GWPCARE4): a randomised, double-blind, placebo-controlled phase 3 trial. *Lancet* 2018;391:1085–1096.
- Arroyo S. Rufinamide. *Neurotherapeutics* 2007;4:155–162.
- Brodie MJ, Rosenfeld WE, Vazquez B, et al. Rufinamide for the adjunctive treatment of partial seizures in adults and adolescents: a randomized placebo-controlled trial. *Epilepsia* 2009;50:1899–1909.
- Biton V, Krauss G, Vasquez-Santana B, et al. A randomized, double-blind, placebo-controlled, parallel-group study of rufinamide as adjunctive therapy for refractory partial-onset seizures. *Epilepsia* 2011;52:234–242.
- Panebianco M, Prabhakar H, Marson AG. Rufinamide add-on therapy for refractory epilepsy. *Cochrane Database Syst Rev* 2018;4:CD011772.
- Thompson AGB, Cock HR. Successful treatment of super-refractory tonic status epilepticus with rufinamide: first clinical report. *Seizure* 2016;39:1–4.
- Wheless JW, Vazquez B. Rufinamide: a novel broad-spectrum anti-epileptic drug. *Epilepsy Curr* 2010;10:1–6.
- Suter MR, Kirschmann G, Laedermann CJ, et al. Rufinamide attenuates mechanical allodynia in a model of neuropathic pain in the mouse and stabilizes voltage-gated sodium channel inactivated state. *Anesthesiology* 2013;118:160–172.
- Rogawski MA, Löscher W. The neurobiology of antiepileptic drugs. *Nat Rev Neurosci* 2004;5:553–564.

18. Rogawski MA, Porter RJ. Antiepileptic drugs: pharmacological mechanisms and clinical efficacy with consideration of promising developmental stage compounds. *Pharmacol Rev* 1990;42:223–286.
19. Mantegazza M, Curia G, Biagini G, et al. Voltage-gated sodium channels as therapeutic targets in epilepsy and other neurological disorders. *Lancet Neurol* 2010;9:413–424.
20. Kuo C-C, Bean BP. Slow binding of phenytoin to inactivated sodium channels in rat hippocampal neurons. *Mol Pharmacol* 1994;46:716–725.
21. Kuo C-C, Lu L. Characterization of lamotrigine inhibition of Na⁺ channels in rat hippocampal neurons. *Br J Pharmacol* 1997;121:1231–1238.
22. Kuo C-C, Chen R-S, Lu L, Chen R-C. Carbamazepine inhibition of neuronal Na⁺ currents: quantitative distinction from phenytoin and possible therapeutic implications. *Mol Pharmacol* 1997;51:1077–1083.
23. Qiao X, Sun G, Clare JJ, et al. Properties of human brain sodium channel α -subunits expressed in HEK293 cells and their modulation by carbamazepine, phenytoin and lamotrigine. *Br J Pharmacol* 2014;171:1054–1067.
24. Jung S, Jeong Y, Jeon D. Epileptic activity during early postnatal life in the AY-9944 model of atypical absence epilepsy. *Cell Calcium* 2015;57:376–384.
25. Cortez MA, McKlerie C, Snead OC 3rd. A model of atypical absence seizures: EEG, pharmacology, and developmental characterization. *Neurology* 2001;56:341–349.
26. Chan KF, Jia Z, Murphy PA, et al. Learning and memory impairment in rats with chronic atypical absence seizures. *Exp Neurol* 2004;190:328–336.
27. Jung S, Seo JS, Kim BS, et al. Social deficits in the AY-9944 mouse model of atypical absence epilepsy. *Behav Brain Res* 2013;236:23–29.
28. Shimada T, Yamagata K. Pentylentetrazole-induced kindling mouse model. *J Vis Exp* 2018;136:56573.
29. Van Erum J, Van Dam D, De Deyn PP. PTZ-induced seizures in mice require a revised Racine scale. *Epilepsy Behav* 2019;95:51–55.
30. Castel-Branco MM, Falcão AC, Figueiredo IV, Caramona MM. Lamotrigine pharmacokinetic/pharmacodynamic modelling in rats. *Fundam Clin Pharmacol* 2005;19:669–675.
31. Castel-Branco M, Lebre V, Falcão A, et al. Relationship between plasma and brain levels and the anticonvulsant effect of lamotrigine in rats. *Eur J Pharmacol* 2003;482:163–168.
32. Walker MC, Tong X, Pery H, et al. Comparison of serum, cerebrospinal fluid and brain extracellular fluid pharmacokinetics of lamotrigine. *Br J Pharmacol* 2000;130:242–248.
33. Perucca E, Cloyd J, Critchley D, Fuseau E. Rufinamide: clinical pharmacokinetics and concentration–response relationships in patients with epilepsy. *Epilepsia* 2008;49:1123–1141.
34. Richens A. Clinical pharmacokinetics of phenytoin. *Clin Pharmacokinet* 1979;4:153–169.
35. Sherwin AL, Eisen AA, Sokolowski CD. Anticonvulsant drugs in human epileptogenic brain. Correlation of phenobarbital and diphenylhydantoin levels with plasma. *Arch Neurol* 1973;29:73–77.
36. Bertilsson L. Clinical pharmacokinetics of carbamazepine. *Clin Pharmacokinet* 1978;3:128–143.
37. Panday DR, Panday KR, Basnet M, et al. Therapeutic drug monitoring of carbamazepine. *Int J Neurorehabilitation Eng* 2017;4:245.
38. Montouris GD, Wheless JW, Glauser TA. The efficacy and tolerability of pharmacologic treatment options for Lennox-Gastaut syndrome. *Epilepsia* 2014;55:10–20.
39. Motte J, Trevathan E, Arvidsson JF, et al. Lamotrigine for generalized seizures associated with the Lennox-Gastaut syndrome. *N Engl J Med* 1997;337:1807–1812.
40. Gáll Z, Vancea S, Szilágyi T, et al. Dose-dependent pharmacokinetics and brain penetration of rufinamide following intravenous and oral administration to rats. *Eur J Pharm Sci* 2015;68:106–113.
41. Meirinho S, Rodrigues M, Fortuna A, et al. Novel bioanalytical method for the quantification of rufinamide in mouse plasma and tissues using HPLC-UV: a tool to support pharmacokinetic studies. *J Chromatogr B Analyt Technol Biomed Life Sci* 2019;1124:340–348.
42. Moavero R, Cusmai R, Specchio N, et al. Rufinamide efficacy and safety as adjunctive treatment in children with focal drug resistant epilepsy: the first Italian prospective study. *Epilepsy Res* 2012;102:94–99.
43. Yaari Y, Beck H. "Epileptic neurons" in temporal lobe epilepsy. *Brain Pathol* 2002;12:234–239.
44. Blumenfeld H, Rivera M, McNally KA, et al. Ictal neocortical slowing in temporal lobe epilepsy. *Neurology* 2004;63:1015–1021.
45. Serafini R, Loeb JA. Enhanced slow waves at the periphery of human epileptic foci. *Clin Neurophysiol* 2015;126:1117–1123.
46. Yang YC, Wang G-H, Chuang A-Y, Hsueh S-W. Perampamil reduces paroxysmal depolarizing shift and inhibitory synaptic input in excitatory neurons to inhibit epileptic network oscillations. *Br J Pharmacol* 2020;177:5177–5194.
47. Wang G-H, Chou P, Hsueh S-W, et al. Glutamate transmission rather than cellular pacemaking propels excitatory-inhibitory resonance for ictogenesis in amygdala. *Neurobiol Dis* 2020;148:105188.
48. Chou P, Wang G-H, Hsueh S-W, et al. Delta-frequency augmentation and synchronization in seizure discharges and telencephalic transmission. *iScience* 2020;23:101666.
49. Steriade M. Interneuronal epileptic discharges related to spike-and-wave cortical seizures in behaving monkeys. *Electroencephalogr Clin Neurophysiol* 1974;37:247–263.
50. Steriade M, Oakson G, Diallo A. Cortically elicited spike-and-wave afterdischarges in thalamic neurons. *Electroencephalogr Clin Neurophysiol* 1976;41:641–644.
51. Blumenfeld H. Cellular and network mechanisms of spike-wave seizures. *Epilepsia* 2005;46:21–33.
52. Bazhenov M, Timofeev I, Fröhlich F, Sejnowski TJ. Cellular and network mechanisms of electrographic seizures. *Drug Discov Today Dis Model* 2008;5:45–57.
53. Speckmann E-J, Elger CE. Introduction to the neurophysiological basis of the EEG and DC potentials. In: Niedermeyer E, Lopes da Silva F, eds. *Electroencephalography: basic principles, clinical applications, and related fields*. 3rd ed. Philadelphia, PA: Lippincott Williams & Wilkins, 1993:15–27.
54. Steriade M. Cellular substrates of brain rhythms. In: Niedermeyer E, Lopes da Silva F, eds. *Electroencephalography: basic principles, clinical applications, and related fields*. 3rd ed. Philadelphia, PA: Lippincott Williams & Wilkins, 1993:28–75.
55. Errington AC, Stöhr T, Heers C, Lees G. The investigational anticonvulsant lacosamide selectively enhances slow inactivation of voltage-gated sodium channels. *Mol Pharmacol* 2008;73:157–169.
56. Holtkamp D, Opitz T, Niespodziany I, et al. Activity of the anticonvulsant lacosamide in experimental and human epilepsy via selective effects on slow Na⁺ channel inactivation. *Epilepsia* 2017;58:27–41.
57. Peng Y-S, Wu H-T, Lai Y-C, et al. Inhibition of neuronal Na⁺ currents by lacosamide: differential binding affinity and kinetics to different inactivated states. *Neuropharmacology* 2020;179:108266.
58. Llinás RR, Walton KD, Lang EJ. Cerebellum. In: Shepard GM, ed. *The synaptic organization of the brain*. Oxford, UK: Oxford University Press, 2004:271–309.
59. Ben-Menachem E, Grebe HP, Terada K, et al. Long-term safety and efficacy of lacosamide and controlled-release carbamazepine monotherapy in patients with newly diagnosed epilepsy. *Epilepsia* 2019;60:2437–2447.